Carbohydrate Polymers 352 (2025) 123156

Contents lists available at ScienceDirect

Carbohydrate Polymers

journal homepage: www.elsevier.com/locate/carbpol

Investigating the interactions between a poloxamer and TEMPO-oxidised cellulose nanocrystals

Alessandra Lavoratti [a], Onajite Abafe Diejomaoh [a], Annela M. Seddon [b], Todor T. Koev [c], Yaroslav Z. Khimyak [c], Robert L. Harniman [d], Katri S. Kontturi [e], Tekla Tammelin [e], Stephen J. Eichhorn [a,*]

[a] Bristol Composites Institute, School of Civil, Aerospace, and Design Engineering, University of Bristol, University Walk, Bristol BS8 1TR, UK
[b] School of Physics, HH Wills Laboratory, University of Bristol, Tyndall Avenue, Bristol BS8 1TL, UK
[c] School of Chemistry, Pharmacy and Pharmacology, University of East Anglia, Norwich Research Park, NR4 7TJ, UK
[d] School of Chemistry, University of Bristol, Bristol BS8 1TS, UK
[e] Sustainable Products and Materials, VTT Technical Research Centre of Finland, FI-02044 Espoo, Finland

ARTICLE INFO

Keywords:
Cellulose nanocrystals
TEMPO oxidation
Adsorption
Triblock copolymer

ABSTRACT

Cellulose nanocrystals (CNCs) have emerged as promising, sustainable materials, with applications in sensors, coatings, pharmaceuticals, and composites. Their modification with block copolymers such as PEO-PPO-PEO triblock copolymers of the Pluronic family has been attempted many times in the literature, with claims that such modification would happen by an anchor(PEO)-buoy(PPO)-anchor(PEO) mechanism. However, there is much disagreement in the literature on this. We herein physically adsorbed Pluronic F127, a nontoxic triblock copolymer poloxamer, comprising hydrophilic polyethylene oxide (PEO) and hydrophobic polypropylene oxide (PPO) blocks, onto the surface of TEMPO oxidised CNCs by simple mixing in an aqueous medium. The adsorption of F127 onto the surface of these CNCs was successful and persistent even after solubilisation. The thermal stability of modified TOCNCs increased (by ~19 °C) compared to their neat and oxidised counterparts. F127-TOCNC suspensions exhibited comparable viscosity to their neat and oxidised counterparts without premature gelation of F127. NOESY NMR observations showed that PPO blocks are more proximal to the TOCNC than the PEO blocks. AFM and QCM-D analyses supported the formation of a rigid, thin layer of block copolymer surrounding the TOCNC. A degree of modification (7 %) was achieved, even after washing, proving that adsorption is persistent and mainly irreversible.

1. Introduction

Cellulose nanomaterials (CNMs) have emerged as attractive alternatives to common synthetic nanofillers due to their highly functionalizable surface and nanoscale size (Foster et al., 2018) as well as their availability, renewability, and potential biodegradability (Eichhorn et al., 2022). As such, research on CNMs spans many fields such as materials science and engineering (polymer composites, adhesives, membranes, textiles, flexible and transparent films, textiles), and medicine (drug delivery, tissue engineering scaffolds, hydrogels) (Eichhorn et al., 2022; Foster et al., 2018). Cellulose nanocrystals (CNCs), one form of CNMs, are highly crystalline rod-shaped nanoparticles, with widths ranging from 3 and 50 nm, and lengths of 50 nm up to 350 nm (Foster et al., 2018; Solhi et al., 2023). CNCs are usually prepared using a top-down process of acid-catalysed hydrolysis. This hydrolysis process targets the disordered regions of the cellulose structure, where the water most typically resides, leaving the most ordered, crystalline regions intact (Llàcer Navarro et al., 2021; Solhi et al., 2023). CNCs prepared using sulfuric acid hydrolysis introduce sulfate half-ester groups that impart a negative charge, colloidally stabilising them in aqueous solutions; these groups are susceptible to degradation and can be removed under mild alkaline conditions (Fraschini et al., 2017; Habibi et al., 2006). TEMPO-mediated oxidation of CNCs produces carboxylic groups on their surfaces, which are less labile compared to sulfate half-ester groups (Fraschini et al., 2017; Habibi et al., 2006). Another advantage of the oxidation of CNCs with TEMPO is that an increase in carboxylic groups may be favourable to their subsequent modification. These modifications include polymer adsorption. This can be achieved by

* Corresponding author.
E-mail address: s.j.eichhorn@bristol.ac.uk (S.J. Eichhorn).

https://doi.org/10.1016/j.carbpol.2024.123156
Received 23 August 2024; Received in revised form 12 December 2024; Accepted 13 December 2024
Available online 15 December 2024

taking advantage of the highly negatively charged surface from TEMPO oxidation, thereby favouring electrostatic adsorption (Llàcer Navarro et al., 2021; Solhi et al., 2023). TEMPO-oxidised celluloses are also known to possess increased hydrophilicity, compared to other forms and derivatives, due to their highly charged surface (Isogai et al., 2011; B. Li et al., 2015).

Surface modification of CNCs via adsorption of block copolymers is a non-covalent strategy that can be carried out in aqueous media. Both these aspects are highly advantageous in the context of CNMs because it does not compromise their physical integrity (Arumughan et al., 2021). Amphiphilic block copolymers comprising both hydrophilic and hydrophobic blocks such as poloxamers – commercially known as Pluronics – have emerged in recent times as they are water soluble while also maintaining one hydrophobic block that can interact with other hydrophobic particles and polymers alike. CNCs possess a quite heterogenous surface, abundant with functional groups and surface charges; all of these contribute in different ways to the adsorption mechanisms of nonionic block copolymers (Arumughan et al., 2021). Moreover, the properties of block copolymers are highly dependent on the concentration and temperature of the system, most notably in the way they self-assemble (Arranja et al., 2016; Carrera Espinoza et al., 2021; Sarkar & Alexandridis, 2012). While this may be an issue to applications that rely on their self-assembly and thermoresponsive behaviour, such as hydrogels for drug delivery, by avoiding premature self-assembly and micelle formation, the adsorption of unimer structures – that is, individual chains – are favoured. Retention of the unimer form could facilitate the adsorption of triblock copolymers in an anchor (PEO)-buoy (PPO)-anchor(PEO) mechanism, as has previously been suggested (Y. Li et al., 2011).

The use of PEO-PPO-PEO block copolymers in conjunction with cellulose-based materials has been studied in the literature for a number of applications, ranging from hydrogels for drug delivery, tissue engineering, ophthalmic interventions (Boonrat et al., 2021; Gutierrez et al., 2017; Orasugh et al., 2019; Tercjak et al., 2015) and composites (Builes et al., 2013; Nagalakshmaiah et al., 2016). More recently, the use of Pluronic F127 has been reported for the gelation of CNCs (Kushan & Senses, 2021) and for the modification of cellulose acetate mats to facilitate electrospinning (Gomez-Hermoso-de-Mendoza et al., 2023). In this sense, the use of Pluronic F127 ($PEO_{99}PPO_{56}PEO_{99}$) for the modification of CNCs is fairly recent. Benefits in doing so lie in an increased thermal stability and the possibility to increase the compatibility of nanocelluloses with polymer matrices in composites (Builes et al., 2013; Nagalakshmaiah et al., 2016). Compared to other block copolymers of the Pluronic family, for example F108 ($PEO_{132}PPO_{50}PEO_{132}$) and F68 ($PEO_{80}PPO_{30}PEO_{80}$), F127 has a larger number of PPO blocks, with 56 PPO units and 99 PEO units which could theoretically interact with hydrophilic surfaces (Cohen et al., 2022; Khaliq et al., 2023). This could be advantageous to increase their compatibility with polymer matrices.

When it comes to nonionic block copolymers that undergo self-assembly, the literature seems to contain fundamental disagreements as to whether it is poly(ethylene oxide) (PEO) or poly(propylene oxide) PPO blocks that effectively adsorb onto cellulose surfaces. These disagreements seem to be related to the complex nature of the surface functionalities of cellulose (Arumughan et al., 2021) and how they interact with water (Solhi et al., 2023). In addition, the F127 poloxamer is known to self-assemble and form micelles above a critical micellization temperature (CMT) and concentration – critical micelle concentration (CMC) (Russo et al., 2024). When the temperature is raised above the CMT, for example, PPO blocks are able to collapse onto the cellulose chains, though the interaction is said to be weak and not governed by electrostatics (Kushan & Senses, 2021).

Nagalakshmaiah et al. (2016) studied the adsorption of Pluronic F127 onto sulfated CNCs for their use in polyethylene melt-processed composites. The authors claimed successful adsorption when using a concentration of 5 wt% content of F127 on CNCs in solution by observing shape changes in functionalised CNCs via SAXS; the mechanism was deemed to be due to hydrophilic/hydrophobic interactions of PEO blocks with the surface of the CNCs. Previous studies have also investigated the adsorption of single block PEO/PEG copolymers onto the surface of cellulose, and concluded, by using Quartz Crystal Microbalance (QCM) measurements, that hydrogen bonding plays an integral role in this process (Bardet et al., 2015; Cheng et al., 2015). Cohen et al. concluded that both Pluronic F127 and F108 adsorb on the surface of CNCs by observing a reduction in the zeta potential of the neat CNCs and the ternary F127/F108/CNC mixtures, along with observing an increase in their widths. It is important to highlight that, in all aforementioned studies, concentrations of up to 20 wt% F127 were used to facilitate self-assembly and co-assembly of CNCs and F127, particularly for applications in thermoresponsive hydrogels. Li et al. (2011) studied the adsorption of $PEO_{19}PPO_{29}PEO_{19}$ on cellulose, polypropylene and polyethylene surfaces, and concluded that PEO blocks have a higher affinity for hydrophilic surfaces than PPO blocks and that an anchor (PEO)-buoy(PPO)-anchor(PEO) mechanism was proposed for hydrophilic cellulose (Li et al., 2011). Tarhanlı and Senses (2023) proposed that the hydrophilic PEO groups of Pluronic L121 (PEO_5PPO_{62}-PEO_5) are adsorbed on CNCs, and instead of a bridging effect, they sterically stabilised the suspension. They also mentioned that the adsorption of PPO blocks to CNCs was only favoured when the suspensions were heated above their phase transition temperature – ranging from 10 to 20 °C as measured from the melting peak from DSC. The authors attributed this behaviour to the strong interaction of PPO blocks with hydrophobic sections of the CNCs above the CMT. This is expected to occur along the ⟨100⟩ edge of the CNCs (Reid et al., 2017). Reid et al. (2017) studied the role of hydrogen bonding in nonionic polymer adsorption to CNCs and silica colloids. The authors emphasized that, in the absence of water, adsorption of PEG to cellulose is likely. However, they argue that adsorption of amphiphilic polymers to CNCs occurs not because of PEG adsorption, but via hydrophobic effects in which the hydrophobic portion of the polymer adsorbs to the surface of CNCs to limit water interactions. In short, even though the literature is abundant with studies reporting the adsorption of PEO-PPO-PEO block copolymers onto cellulose surfaces, many conflicting statements are made on both the structure of the block copolymers or on the ratio of hydrophobic PPO and hydrophilic PEO blocks present. The majority of the literature seems to agree that adsorption occurs, though some conflicting reports on the nature of this adsorption still remain, particularly for poloxamers such as F127. These conflicts seem to stem from whether PEO or PPO blocks are closer to cellulose surfaces, or even the nature of the interaction. With this, our hypothesis is that even though persistent adsorption might occur, these interactions could be far more complex and even involve the effects of the presence of water. This could have implications in gel formation mechanisms of composite CNC/poloxamers, thermoresponsive gels for drug delivery, and other applications.

2. Experimental

2.1. Materials

Pluronic F127, a triblock copolymer PEO_{99}-PPO_{56}-PEO_{99}, supplied by Merck (Dorset, UK) was used (molecular weight = 12,600 g mol^{-1}). Commercial sulfated cellulose nanocrystals (SCNC) were obtained from the University of Maine (Orono, MA, USA) at a 11.5 wt% solids content (molecular weight = 6675 g mol^{-1}). 2,2,6,6-Tetramethylpiperidine 1-oxyl (TEMPO), sodium bromide (NaBr) and ethanol (99.8 %) were supplied by Merck (Gillingham, UK) and sodium hypochlorite (NaClO) and sodium hydroxide (NaOH) were supplied by Fisher Scientific (Leicestershire, UK). All reagents were used as received without purification. Deionised water was used for all experiments.

2.2. TEMPO-mediated oxidation of cellulose nanocrystals

The TEMPO-mediated oxidation of CNCs was adapted from a

previously described method (Fraschini et al., 2017; Isogai et al., 2011). Briefly, 3 g (dry weight) of CNCs was dissolved in ultrapure water to obtain a 1 wt% suspension. 0.048 g (0.1 mmol g^{-1}-CNCs) of TEMPO/NaBr and 0.3 g (1 mmol g^{-1}-CNCs) were added to the suspension and stirred until dissolution occurred (for ~2 h). The pH of the suspension was adjusted to 10–11 with 0.5 M NaOH after the addition of TEMPO/NaBr and prior to the addition of NaClO. After that, NaClO (10 mmol/g-CNCs) was slowly added dropwise to the suspension over the course of 1 h, yielding a viscous, yellow suspension. The pH of the suspension was continuously adjusted to 10–11 until no further decrease was observed. The pH was continuously monitored with a pH meter (FiveGo Mettler Toledo portable pH meter, model F2; Mettler Toledo, Ohio, United States). Care was taken to keep the pH close to 10.5. To ensure that, only a few drops of NaOH 0.5 M were added. Upon completion, the reaction was quenched with 30 mL of ethanol (1 ml/0.1 g-CNC) whereupon the suspension turned white. This TEMPO-oxidised CNC suspension (TOCNC) was centrifuged three times at 10,000 rpm for 20 min and washed with deionised water. The final pH of the TOCNC suspension was 6. The suspension was then stored in a fridge at 4 °C.

2.3. Adsorption of Pluronic F127 to TOCNCs

A simple mixing procedure was used to adsorb the triblock copolymer F127 to the TOCNCs. Firstly, a 1 wt% concentration of F127 was slowly dissolved in deionised water for 2 h at 6 °C with the aid of an ice bath. Then, the F127 suspension was gradually added to a TOCNC suspension (1 wt%) and slowly stirred for an additional 2 h using magnetic stirring. This F127-TOCNC suspension was stored at 4 °C. The concentrations were chosen to keep F127 in its unimer form, to better evaluate adsorption and to minimize the amount of polyoxamer for their application in the aqueous processing of polymer composites, following the work of Nagalakshmaiah et al. (2016). Additionally, the ratio of 1:1 F127:TOCNC represents the weight percentage of each component, following the same mixing and adsorption procedure mentioned in earlier studies (Kushan & Senses, 2021; Nagalakshmaiah et al., 2016).

2.4. Characterization

2.4.1. Fourier-transform infrared spectroscopy

Functional groups and the presence of triblock-copolymer on the CNCs were investigated using a FTIR spectrophotometer in attenuated total reflectance (ATR) mode on air-dried samples. Spectra were collected from 4000 cm^{-1} to 400 cm^{-1} and 8 scans were performed.

2.4.2. Conductometric titration

The surface charge of SCNCs and TOCNCs was measured by conductometric titration. 0.05 wt% of SCNCs or TOCNCs were redispersed and dialysed against deionised water for 3 days to remove free sodium ions. A Dowex Marathon C hydrogen cation exchange resin was used to exchange counterions to protons prior to the measurements. An amount of 12 g of resin per 1 g CNC was used following a methodology described by Li et al. (2020). The resin was then added to the suspension and vigorously stirred for 2 h. Upon protonation, the resin was removed and 1 ml 100 mM NaCl was added to the suspension to increase the reading range. The suspension was titrated with 100 µl additions of 10 mM NaOH following a procedure recommended by Foster et al. (2018). The titration curve was obtained by plotting the conductivity of the CNC suspension against the volume of NaOH (Supplementary Material).

2.4.3. Zeta potential measurements

Zeta potential measurements were performed on aqueous suspensions dispersed at 1 mg ml^{-1} using a Zetasizer Nano-ZS with a DTS 1070 capillary cell. Measurements were obtained at 25 °C, using a refractive index of water 1.33. In total, 3 measurements were taken per sample with 50 runs per measurement. Average values with their respective standard deviations are reported.

2.4.4. Thermogravimetric analysis

The thermal stability of air dried samples was evaluated using a Netzsch STA 449 Jupiter F3 instrument, with a heating range from 30 to 800 °C at a rate of 10 °C min^{-1} under a nitrogen flow of 50 ml min^{-1}. 10 mg of sample was used. DTG curves were obtained from the percentage loss data from the TGA using Proteus Analysis software (version 6.1).

2.4.5. Differential scanning calorimetry

The thermal transitions of the samples were investigated by differential scanning calorimetry using TA Instruments Discovery DSC 2500 equipment. 5 mg of sample was placed in TZero hermetic aluminium pans and heated at a rate of 10 °C/min using a heating cycle from 30 °C to 200 °C. and a subsequent cooling cycle from 200 °C to −50 °C. The specific enthalpy values were obtained from the area under the first melting peak. The degree of crystallinity, as a percentage, of the samples containing F127 was calculated using the equation

$$X_c = \frac{\Delta H_m}{\Delta H_{m,0}} \times 100\% \quad (1)$$

where ΔH_m is the melting enthalpy obtained from the first heating ramp and $\Delta H_{m,0}$ is the melting enthalpy of fully crystalline F127; this was taken to be 229.1 J g^{-1} using literature values (Shaker et al., 2020; Tenorio-Alfonso et al., 2023).

2.4.6. Rheology

Rheological measurements were carried out using a TA Instruments DHR Rheometer and a 40 mm serrated parallel Peltier plate to avoid 'wall slippage' (Bertula et al., 2019). The samples were concentrated to a 10 wt% solids content due to equipment limitations. The samples were then subjected to a pre-shear regime from 0.001 to 100 rad s^{-1} to determine the linear viscoelastic region (LVR) and later rested for 10 min using a time sweep at 1 Hz and 0.25 % strain. All experiments were carried out at room temperature (25 ± 1 °C).

2.4.7. Transmission Electron Microscopy (TEM)

The morphologies of the unmodified and modified CNCs were captured using a JEOL JEM-1400 TEM in bright field mode with an accelerating voltage of 120 kV. The CNC-containing samples were diluted to 0.001 wt% before imaging. The sizes of the CNCs were measured using ImageJ. Their dimensions were represented using a box plot using Origin 2020b. Statistical analysis was performed using a two sample mean *t*-test with $p < 0.05$ ($n = 30$).

2.4.8. Small Angle X-ray Scattering (SAXS)

SAXS experiments were performed on a Ganesha SAXS/WAXS instrument (Xenocs) fitted with a Cu Kα microfocus source (1.544 Å). Samples were prepared at 1 wt% at 25 °C. 50 µL samples were placed in a 1.5 mm borosilicate glass capillary (Capillary Tube Supplies Ltd) and sealed using a UV cured epoxy (Norland). Data were collected over a q range of $0.007 \leq q \leq 0.25$ $Å^{-1}$ for an exposure time of 3600 s. A blank capillary and water background were subtracted from all data. Data were reduced using SAXSGUI and subsequent processing was carried out using SASView.

2.4.9. Solid-state nuclear magnetic resonance (ssNMR)

^{1}H-^{13}C cross-polarisation magic angle spinning (CP/MAS) NMR was performed on freeze-dried samples on a Bruker Avance III NMR spectrometer operating at a ^{13}C frequency of 75.21 MHz. The samples were packed into an 80-uL rotor and spun at a magic angle spinning (MAS) rate of 10 kHz. All ssNMR spectra were acquired using ^{1}H $\pi/2$ *rf* pulse of 3.2 µs, contact time of 2 ms, recycle delay of 10 s, and at 20 °C.

Global spectral deconvolution was carried out using the MestreLab MNova (v14.2) package.

The degree of surface oxidation of TOCNC and the surface adsorption of F127 was calculated according to the equation

$$DSM\% = \frac{A_{\text{modification}}}{n \times A_{(C4s+C6s)}} \times 100 \quad (2)$$

where $A_{\text{modification}}$ is the area under the deconvoluted CH_3 peak in PPO (ca. 18.6 ppm) of the sample, and $A_{(C4s+C6s)}$ is the area under the deconvoluted peaks associated with the cellulose backbone surface moieties of C_4 and C_6 carbons (ca. 85 an 63 ppm, respectively).

2.4.10. Pulsed-field gradient (PFG) spectroscopy and nuclear Overhauser effect spectroscopy (NOESY)

F127-TOCNC, TOCNC, and F127 were solubilised in D_2O, and their diffusion was measured using Bruker's '*stebpgp1s*' pulse sequence, using gradient pulse of 7 ms, and diffusion time of 0.16 s, 64 points, recycle delay of 2 s, a minimum of 16 scans and acquired at 20 °C, achieving maximum signal attenuation of 98 %. The decay of signal intensity as a function of gradient strength was fitted to the Stejskal-Tanner equation

$$I_G = I_{G=0} exp\left[-(\gamma \delta G)^2 D\left(\Delta - \frac{\delta}{3}\right)\right] \quad (3)$$

where $I_{G=0}$ is the signal intensity at a gradient strength of zero, G is the gradient strength, D is the self-diffusion coefficient, δ is the gradient pulse duration, and Δ is the diffusion time. NOESY NMR was recorded using Bruker's '*noesygpphpp*' pulse sequence, using mixing times of 0.5–2 s, 64 points and recycle delay of 2 s. All solution-state NMR experiments were performed on a Bruker Avance NEO spectrometer, equipped with an iProbe, operating at ^1H frequency of 500.23 MHz.

2.4.11. Atomic force microscopy (AFM)

Atomic Force Microscopy characterization was performed in ambient environment using a Multi-mode VIII microscope with Nanoscope V controller operating under PeakForce control. ScanAsyst-Air-HR cantilevers were utilised of nominal tip radius and spring constant of 2 nm and 0.4 N m^{-1} respectively. Samples of F127-TOCNC and TOCNC were deposited to separate cleaved mica sheets at a concentration of 0.0005 wt% and dried for 2 h prior to AFM investigation.

2.4.12. Quartz crystal microgravimetry with dissipation monitoring (QCM-D)

Quartz crystal microgravimetry with dissipation monitoring was used to monitor the interactions between F127 and TOCNC. Silica-covered AT-cut QCM-D sensors with fundamental resonance frequency $f_0 \approx 5$ MHz (Biolin Scientific, Gothenburg, Sweden) were used. The sensor surface was cleaned via UV/ozone treatment followed by adsorption of a thin anchoring layer of branched polyethylene imine (PEI) (Sigma Aldrich). After this, TOCNCs were allowed to adsorb from 3 g l^{-1} aqueous suspension for 25 min, followed by rinsing with water, resulting in a formation of a stable TOCNC layer with a dry an areal mass of ~10.6 mg m^{-2}.

QCM-D measurements were conducted with an E4 Analyzer instrument (Biolin Scientific, Gotherburg, Sweden). In the QCM-D technique, the mass adsorbed on the sensor surface is directly proportional to the detected changes of its resonance frequency (Δf), while the viscoelastic properties of the adsorbing layer correlate with the change in dissipation of energy (ΔD). The dissipation factor D of the oscillating adsorbing layer can be found using the equation

$$D = \frac{E_{\text{diss}}}{2\pi E_{\text{stored}}} \quad (4)$$

where E_{diss} is the energy dissipated during an oscillation cycle, and E_{stored} the total energy stored in the oscillator. When the ΔD value for the adsorbed layer is relatively low, $\leq 1{\cdot}10^{-6}$, the layer can be considered to be elastic, and it is acceptable to estimate the adsorbed dry mass using the Sauerbrey equation (Sauerbrey, 1959)

$$\Delta m = -\frac{C\Delta f}{n}, \quad (5)$$

where C is the sensitivity constant of the device (17.7 ng Hz^{-1} cm^{-2} for a 5 MHz crystal) and n is the overtone number.

Prior to adsorption measurements, the TOCNC film was allowed to stabilize in pure water. After the stabilization of the baseline, adsorption of F127 from 100 mg l^{-1} concentration onto the TOCNC surface was monitored for ~1 h, after which the surface was again rinsed with pure water for ~30 mins. A temperature of 23 °C and a flow rate of 0.1 ml min^{-1} were maintained throughout the measurements. The data presented were acquired using the fifth overtone (25 MHz, $f_0 = 5$ MHz, $n = 5$). Two parallel measurements were recorded. AFM images were obtained using Anasys afm + instrument (Anasys Instruments Inc., Santa Barbara, CA, USA), to determine the morphology of the QCM-D samples. The images were scanned in tapping mode in air at 25 °C using ACTA silicon cantilevers with a spring constant of 37 N m^{-1} (Applied Nanostructures Inc., Mountain View, CA, USA). No image processing except flattening was carried out.

3. Results and discussion

3.1. FTIR analysis of functional groups present on the cellulose nanocrystals

The presence of functional groups on, and adsorbed polymer to, the CNCs was investigated using Fourier Transform Infrared Spectroscopy (FTIR) (Fig. 1). SCNCs showed typical stretching vibrations located at ~3320 cm^{-1} (O—H), ~2900 cm^{-1} (C—H) and ~ 1031 cm^{-1} (C—O) (Onyianta et al., 2022). The appearance of an absorbance band located at ~1607 cm^{-1}, related to the presence of carboxylate groups, is evidence that the TEMPO-oxidation of the CNCs was successful (Kim et al., 2019; Onyianta et al., 2023). The presence of Pluronic F127 displayed a doublet band located at ~2968 and ~ 2900 cm^{-1} related to asymmetric and symmetric aliphatic C—H stretching, respectively, pertaining to the methyl groups of PEO and PPO blocks (Cohen-Erner et al., 2021; Shaker et al., 2020). The bands located at ~1470 cm^{-1} and ~ 1360 cm^{-1} are related to CH_2 wagging between PEO and PPO blocks (Suhail et al., 2022). For F127-adsorbed TOCNC, a band located at ~2968 cm^{-1} was present, which is related to the methyl groups of the block copolymer. The band located at ~2900 cm^{-1} is related to the methyl groups of the PPO blocks and is overlapped by the 2900 cm^{-1} band corresponding to

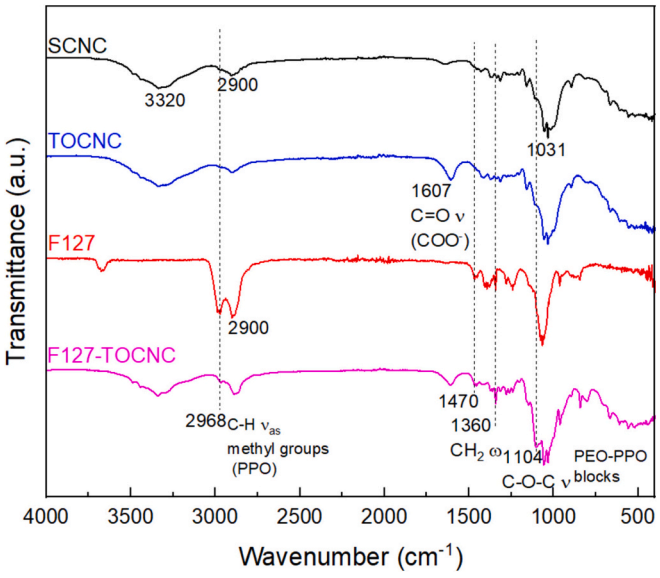

Fig. 1. Typical Fourier Transform Infrared (FTIR) spectra of sulfated cellulose nanocrystals (SCNC), TEMPO-oxidised cellulose nanocrystals (TOCNC), pluronic F127 (F127), and TOCNC with adsorbed F127 (F127-TOCNC). Dotted lines are guides for the eyes only.

the C—H stretching vibrations of cellulose. For F127-TOCNC, the F127 bands were also present at ~1470 cm^{-1} and ~ 1360 cm^{-1}, related to the CH_2 symmetric and asymmetric wagging. The band located at ~1104 cm^{-1} in F127-TOCNC is related to the C-O-C stretching vibration between PEO and PPO blocks (Cohen-Erner et al., 2021; Nagalakshmaiah et al., 2016). This shows that F127 was at least adsorbed onto the surface of TOCNC, though it is not conclusive from this evidence alone which blocks of the copolymer are most proximal to the cellulose chains.

3.2. Surface charge and dimensions of the cellulose nanocrystals

The morphologies and dimensions of the CNC and F127-TOCNC samples were determined using TEM. Representative electron micrographs of the samples are shown in Fig. 2. The mean widths of SCNCs, TOCNCs and F127-TOCNCs are reported in Table 1. Overall, no significant statistical difference was observed between the widths of different CNC samples. Fig. 2a shows a few spherical structures that could be the result of an accumulation of F127 solution upon casting. Smaller micelles in the order of 10 nm could not be observed in TEM micrographs probably due to the fact that the concentration of F127 used in this study was below the critical micellization concentration. This is in line with the usual micelle formation mechanism of nonionic Pluronic F127 block copolymers. For 127, at low concentrations and temperatures – that is, below the critical micellization concentration and temperature – both PPO and PEO are present in aqueous solutions as individual chains (unimers) with a radius of 2 nm. Above the critical micellization temperature and concentration, the self-assembly of F127 micelles in aqueous solution occurs due to the hydrophobic character of PPO chains, which associate to form a dense core whereas PEO blocks stretch out to form a hydrophilic corona. This transition is gradual, and for this reason micelles and unimers can coexist (Branca & D'Angelo, 2019; Ojha et al., 2020; Suman et al., 2021). Suman et al. (2021) mention that the driving force for micellization of F127 itself is entropic in nature: the water molecules around the hydrophobic PPO blocks have a local high order. An increase in temperature results in increased interactions between hydrophobic blocks, 'squeezing' the highly ordered water molecules out of the core formed by the PPO blocks towards the hydrophilic corona or in the bulk aqueous solution, resulting in a gain of entropy (Suman et al., 2021).

Table 1
Surface charge, zeta potential, and widths of sulfated CNCs (SCNC), TEMPO-oxidised CNCs (TOCNC), Pluronic F127 poloxamer (F127), F127 modified TOCNC (F127-TOCNC).

Sample	Surface charge $mmol/kg_{CNC}$	Zeta potential (mV)	Width (nm)
SCNC	448.7 ± 8.3	−31.2 ± 3.5	8.4 ± 1.8
TOCNC	550.0 ± 22.0	−47.6 ± 7.1	10.5 ± 3.1
F127	–	−7.2 ± 1.3	–
F127-TOCNC	–	−19.5 ± 5.8	9.5 ± 2.3

The SCNCs in Fig. 2b exhibited a typical morphology, as did TOCNCs in Fig. 2c. From the images shown in Figs. 2b,c,d, it is noted that the presence of F127 did not alter the shape of the TOCNCs (cf. Fig. 2c&d). As reported in the literature, the critical micellization temperature of F127 is 27 °C at a concentration of 1 wt% (Kumar et al., 2023). This temperature decreases with an increasing F127 concentration which leads to micelle formation at a higher solids content. For F127-TOCNC, free micelles were not observed at the concentration of 0.001 wt% used for casting.

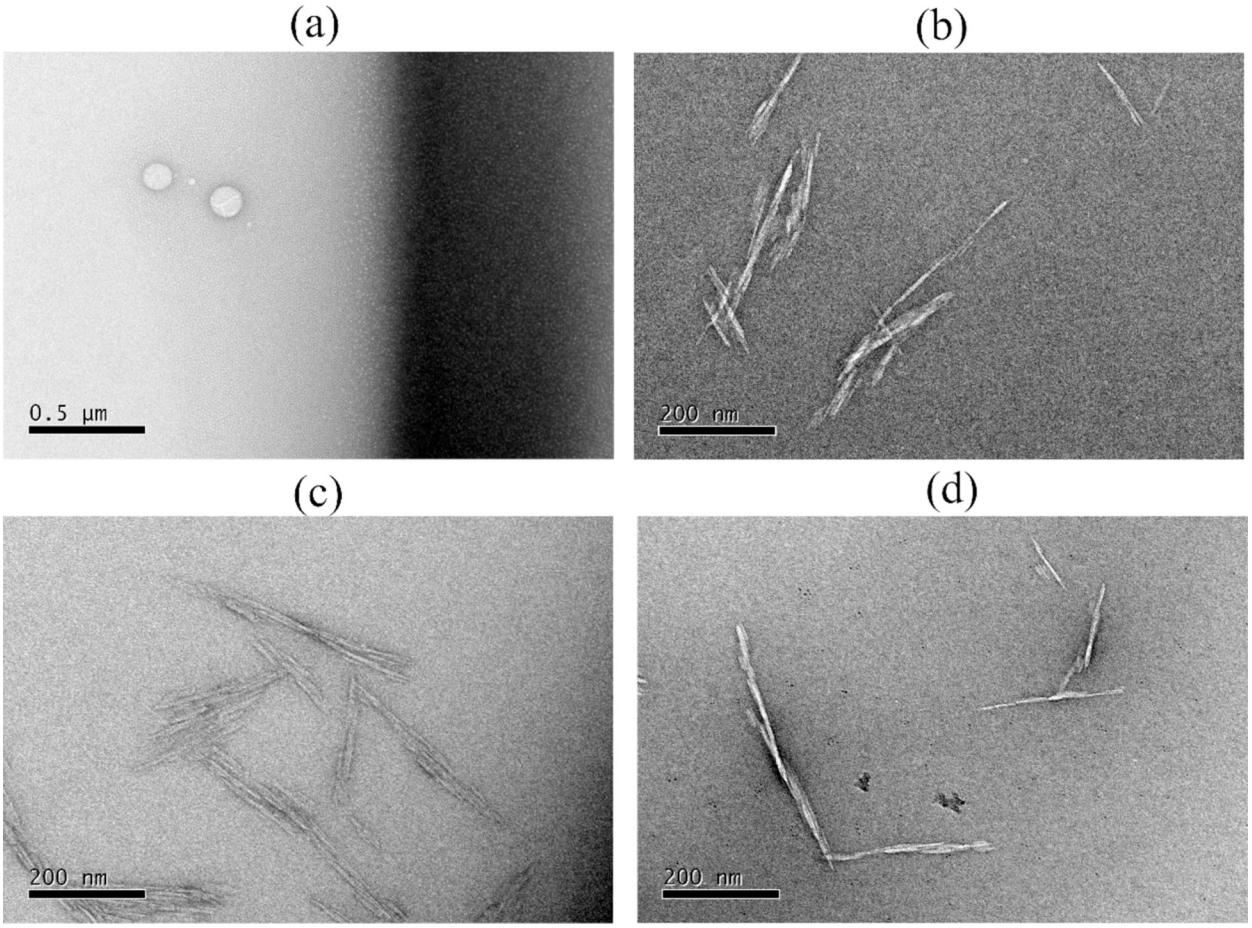

Fig. 2. Typical Transmission Electron Microscope (TEM) images of F127 (a), SCNC (b), TOCNC (c), F127-TOCNC (d).

It is also possible that the surface charges imparted by TOCNC prevented their formation, as has previously been suggested: the mechanism, in this case, was deemed to be driven by changes in the surface tension of the aqueous medium and solution viscosity, which affected the micellization behaviour (Kumar et al., 2023; Mata et al., 2004). If the anchor-buoy-anchor mechanism holds true, this could be advantageous to keep F127 in its unimer conformation and favour anchoring to TOCNC surfaces. With that, a bulk effect of F127 micelles mixed with CNCs could be prevented, whereby they would not actually adsorb to the surface. Moreover, the fact that the size and shape of CNCs was not significantly altered suggests that even though adsorption could have occurred, the unimer chains of F127 could be surrounding TOCNC, where the size difference would be too small to be captured by TEM.

The surface charges (Conductometric titration; Fig. S1) and zeta potentials of the samples are also reported in Table 1. Following TEMPO oxidation, the surface charge of the TOCNCs increased in comparison to SCNCs due to the introduction of negatively charged carboxylate groups at the C6 position of the cellulose chain/rings. These values are in line with the literature for oxidised CNCs: typical values for TEMPO-oxidised CNCs range from 200 to 3500 mmol kg^{-1}_{CNC} (Foster et al., 2018). Comparable values (480 mmol kg^{-1}_{CNC}) were reported by Vanderfleet et al. (2019) for TEMPO-oxidised SCNCs.

The surface charge of the samples was further characterized using zeta potential measurements (Table 1). These data demonstrated that SCNC samples have lower charge potential (~ −31 mV) in comparison to TOCNC (~ −48 mV), which is in line with conductometric titration results. Nonionic block copolymer F127 exhibited a charge potential of −7.2 mV, in accordance with previous literature values (Tarhanlı & Senses, 2023). For F127-TOCNC samples, the charge potential was lower than that of TOCNC. This indicated that when F127 was adsorbed to the surface of TOCNCs it masks some of the surface charges on the sites where it is anchored, even in an aqueous medium. FTIR results demonstrated (Fig. 1) that F127 is present at the surface of the CNCs, so this masking is likely to have been an issue.

Fig. 3 shows the SAXS patterns for F127 and CNC samples. All curves appear similar. The upturn of the data from a flat to a steady gradient at a high to a lower Q occurs in the same position, suggesting the objects causing the scattering are of a similar size (Table S1). The low Q region has a slope of ~ − 2 for SCNC, suggesting a platelet-like shape, whereas TOCNC and F127-TOCNC samples exhibited a slope of ~ − 1.7, suggesting a shape between a rod and a platelet. It also further demonstrates that the adsorption of F127 does not have a major effect on the shape of

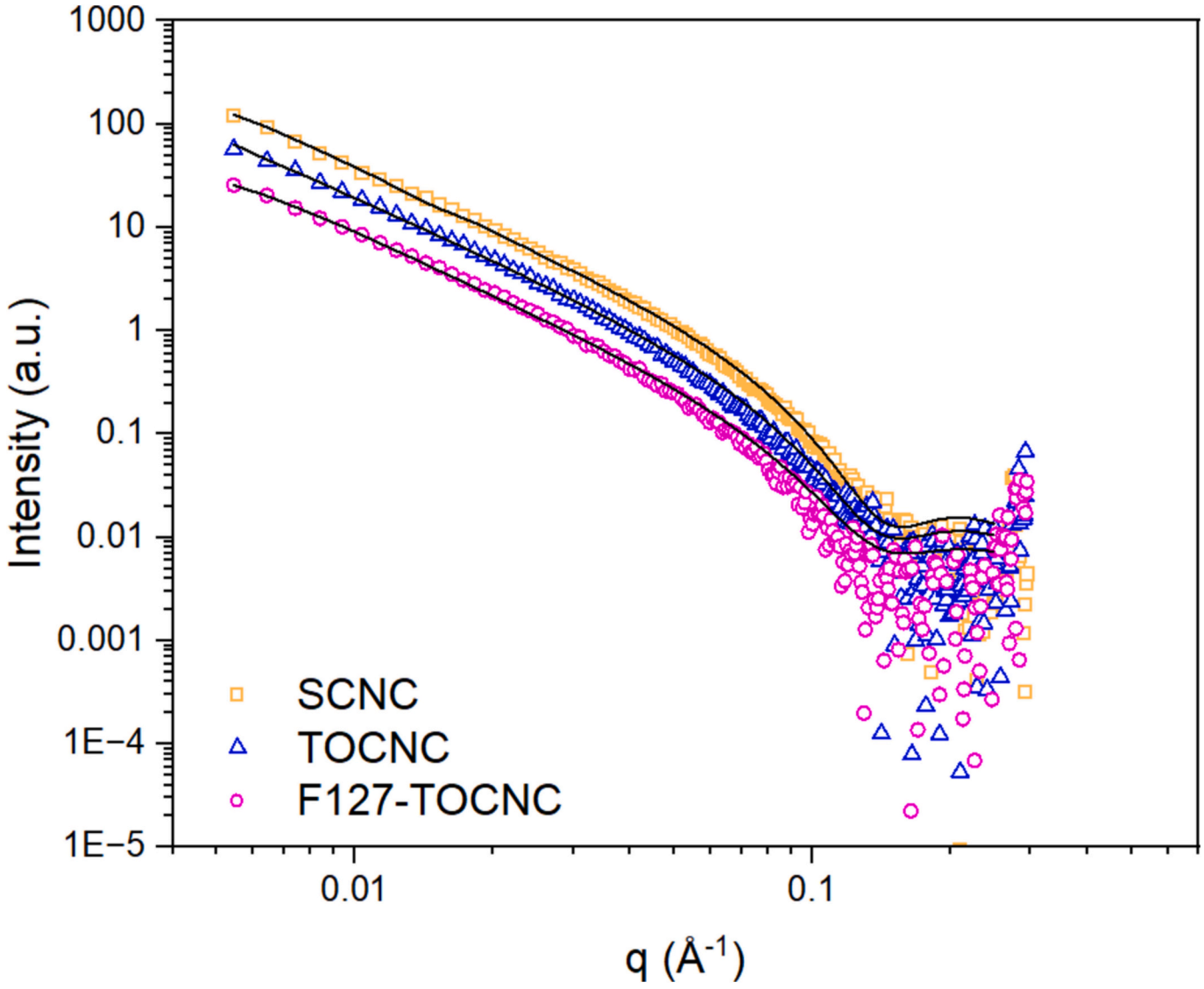

Fig. 3. Typical Small Angle X-ray Scattering (SAXS) curves for sulfated CNCs (SCNC), TEMPO-oxidised CNCs (TOCNC), Pluronic F127 poloxamer (F127) and F127 modified TOCNC (F127-TOCNC). The black lines correspond to the rectangular prism model fitting (fitting data are reported in Supplementary Information, Table S1).

the TOCNCs. In all, the SAXS data are consistent with TEM results with the samples being roughly the same size at first approximation. F127 at 1 wt% did not scatter in the entire Q range. F127 in solution only forms micelles above their critical micellization concentration (CMC) and critical micellization temperature (CMT). As the concentration increases, the micelles are formed at lower temperatures and so the CMT decreases. The samples were analysed at 23 °C, and at a concentration of 1 wt%, well below the CMT and CMC of F127. In addition, F127 unimers in aqueous solution have an approximate size of 9–12 nm (Russo et al., 2024), whereas micelles can have a hydrodynamic diameter of ~15 nm (Kushan & Senses, 2021), which can, if present, be easily detected using SAXS. The lack of any peaks in the SAXS data confirms that no micelles were formed.

3.3. $^{1}H–^{13}C$ CP/MAS NMR

Solid-state NMR was performed to both confirm the adsorption of F127 onto TOCNC, and the nature of the interaction. Fig. 4a shows the ^{1}H – ^{13}C CP/MAS NMR spectra of SCNC, TOCNC, F127 and F127-TOCNC. Both SCNC and TOCNC exhibit peaks corresponding to C1 (105 ppm), C4 (80–90 ppm), C2, C3 and C5 (70–80 ppm) and C6 (60–70 ppm) carbons of the anhydroglucose rings of cellulose (see Fig. 4 and inset). TOCNCs exhibited a peak at 175 ppm corresponding to the C6 from COO^- groups introduced by TEMPO oxidation. This peak is also present for F127-TOCNC. From the TOCNC C6 peak, the degree of oxidation was calculated to be 11.38 %. In theory, about half the primary hydroxy groups of CNCs are accessible to oxidation – the other half are thought to be hidden inside the crystalline core of CNCs and, as such, ~20 % of the total anhydroglucose units can be oxidised (Fraschini et al., 2017). Noting that some of the C6 carbons in sulfated CNCs possess SO^{3-} groups (Batta-Mpouma et al., 2023) and that TEMPO oxidation appears not to displace them, the degree of modification found herein is in line with literature findings.

The methyl group of the PPO block was assigned to the ^{13}C singlet at ca. 18 ppm., whereas the alkyl chains of the PEO blocks assigned to the multiplet at ca. 70–80 ppm on the neat F127 spectrum (Fig. 4b). An overlap between the peaks corresponding to alkyl chains of PEO blocks and the C2, C3 and C5 carbons of TOCNCs can be observed. However,

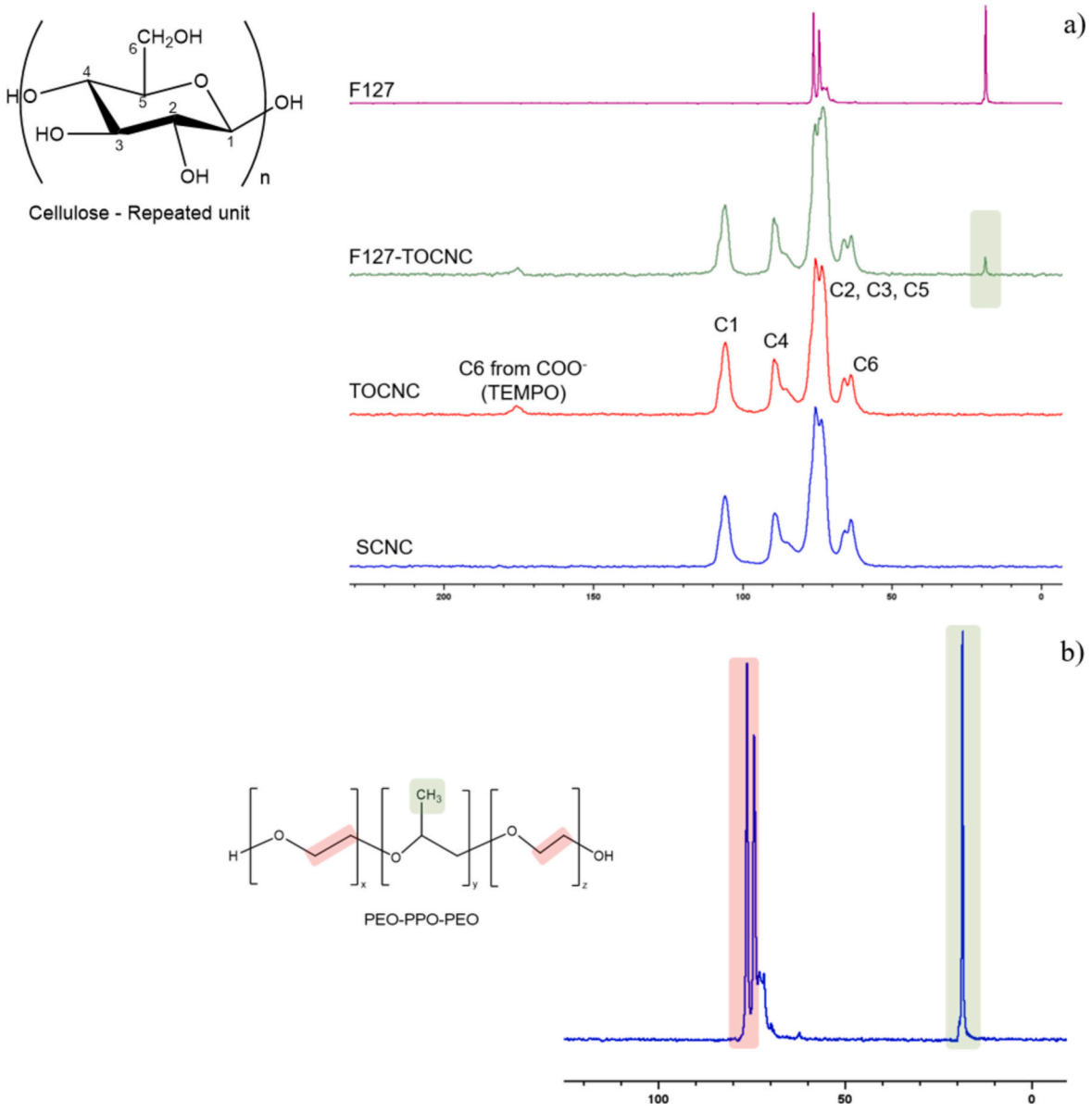

Fig. 4. ^{1}H-^{13}C CP/MAS NMR spectra of sulfated cellulose nanocrystals (SCNC), TEMPO-oxidised cellulose nanocrystals (TOCNC), F127-modified TOCNC (F127-TOCNC), and Pluronic F127 poloxamer (F127), with carbon peak assignment of cellulose and F127.

the peak assigned to the methyl group of the PPO blocks (18 ppm) can be seen in the F127-TOCNC spectrum, evidencing that adsorption to the TOCNC occurred. The degree of modification was calculated from the peak located at 18 ppm; a value of 9.12 % (± 0.4 %) was determined. To resolve whether the adsorption was persistent, freeze-dried F127-TOCNC samples were solubilised in *dd*H_2O, stirred for 24 h, spun down (11,000 ×*g*, 5 min), the supernatant was removed and the resultant pellet freeze-dried overnight. Analogous $^{1}H—^{13}C$ CP/MAS experiments were performed (Fig. S2). This time, the degree of substitution was 7.61 % (± 0.3 %), showing that adsorption is persistent and that only a small percentage of F127 is desorbed from the surface upon washing. It is important to note that washing the unadsorbed F127 provides information on how much block copolymer is desorbed, but it does not confirm which blocks are more proximal.

The self-diffusion coefficients of TOCNC, F127, and F127-TOCNC were calculated to quantify the persistence of the adsorption through solubilisation (Fig. 5). At first it is noted that F127 diffuses much faster than TOCNC or F127-TOCNC, with D = 1.36 E^{-10} m^2/s. Comparable values were found by Ojha et al. (2020) for up to 20 wt% of F127 in aqueous solution, where F127 existed in the form of isotropic micelles in solution, which precedes the ordered phase. In our study, however, no micelle formation was observed due to the concentration and mixing temperature used, which are both well below the critical micellization concentration and temperatures (CMT = 27 °C at 1 wt%). Still, these data confirm that F127 unimers are able to move freely and are not bound by any micelles. This, in turn, should favour the adsorption of F127 to TOCNC as a unimer. It should also make PPO and PEO equally accessible for adsorption to better understand which blocks are closer to TOCNC. The coefficients of diffusion of TOCNC (D = 3.91E^{-13} m^2/s) and F127-TOCNC (D = 4.18E^{-13} m^2/s) are much slower than neat F127, and similar to each other, which indicates that F127 is securely adsorbed and seemingly not desorbed after solubilisation.

Arumughan et al. (2021) recently reviewed the adsorption of ionic and nonionic polymers on cellulose. The authors pointed out that the large number of hydroxy groups on the surface of both cellulose and nonionic copolymers – such as xyloglucans – has led to claims that the driving force for this adsorption is enthalpic. In addition to that, Hanus and Mazeau (2006) also cite molecular dynamic simulations that demonstrated that the adsorption is predominantly governed by polar components such as hydrogen bonding. These models, however, did not explicitly consider water in their simulations. In the presence of water, Arumughan et al. (2021) suggest that hydrogen bonds between nonionic polymers can be substituted by hydrogen bonds with water instead. Reid et al. (2017) first reported that hydrogen bonding between PEG and cellulose does not occur in the wet state. They state that the hydroxy groups on cellulose are not acidic enough to form hydrogen bonds with PEG in the presence of water. Adsorption, in that case, is more likely driven by an entropically favoured release of water from hydrated surfaces – as is the case for many other cellulose nanomaterials (Etale et al., 2023; Solhi et al., 2023), and has been demonstrated and modelled for cellulose-graphene interfaces in the presence of water (Alqus et al., 2015).

To further elucidate the adsorption of F127 to TOCNC, a $^{1}H—^{1}H$ NOESY NMR was carried out on F127-TOCNC (Alqus et al., 2015; Kong et al., 2023); see Fig. 6. This form of spectroscopy provides information about the spatial proximity of protons (up to ca. 3.5 Å). This is useful to determine the relative configuration of molecules or, in this case, to seek information on whether PEO or PPO blocks are more proximal to the TOCNC surface. It is important to note that it does not measure adsorption, quantitatively or qualitatively, nor does it provide any information about the nature of the interactions (i.e., hydrogen, covalent bonding).

An NOE crosspeak was observed between the CH_3 groups of PPO and the ^{1}H of TOCNC at both short (0.5 s) and intermediate (1.0 s) mixing times (crosspeak at ca. 1.04 ppm/3.34 ppm, Fig. 6 red arrow). This suggests that the methyl group is spatially closer to TOCNC than the

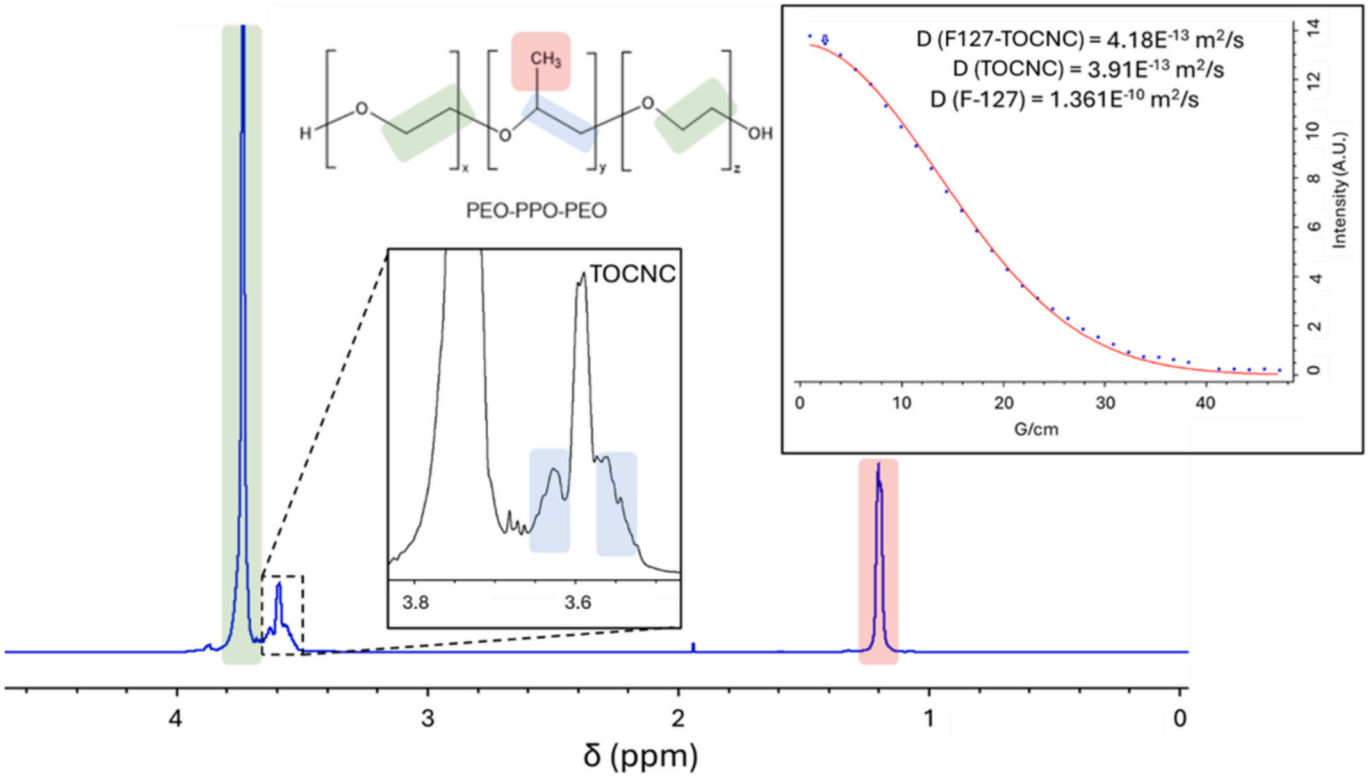

Fig. 5. ^{1}H NMR spectrum of F127-TOCNC, with ^{1}H peak assignment of the CH_3 and C_2H_4 regions of F127 and of TOCNC. Inlay showing an intensity attenuation curve as a function of gradient strength during DOSY NMR, with quantified self-diffusion coefficients (m^2/s) of Pluronic F127 poloxamer (F127), TEMPO-oxidised CNCs (TOCNC) and F127 adsorbed TOCNCs (F127-TOCNC).

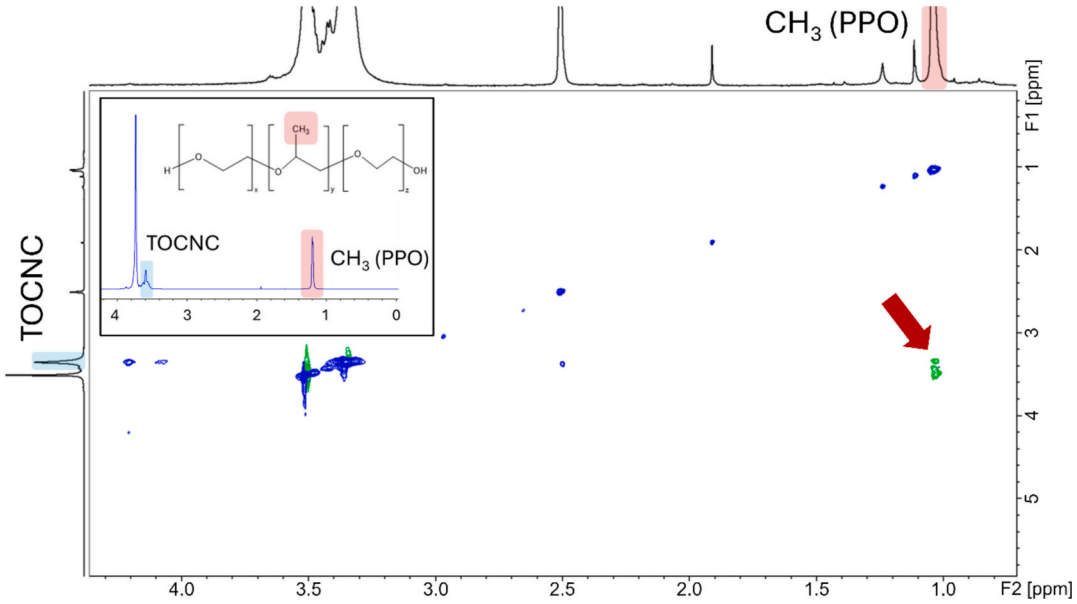

Fig. 6. $^{1}H—^{1}H$ NOESY spectrum of F127-TOCNC in D_2O. PPO protons shown in pink, TOCNC protons shown in blue. Red arrow indicating NOE crosspeak between ^{1}H (CH3, PPO) and ^{1}H (TOCNC).

alkyl chains that comprise the PEO blocks.

AFM results further confirm the formation of a thin layer of block copolymer on the surface of TOCNCs. F127-TOCNCs showed a tight, narrow region of raised adhesion around their periphery (Fig. S3). TOCNCs however show a large extended region of adhesion around their peripheries, which is most likely due to ambient hydration. The changes in the hydrophilic/hydrophobic characteristics are further proof of the successful functionalisation, which in turn is also evidence of the change in the surface charge profile of the TOCNCs after F127 adsorption.

Although several reports suggest that the nature of adsorption could be primarily driven by hydrogen bonding of PEO blocks to CNC surfaces in an anchor-buoy-anchor manner, our results seem to suggest that the simple formation of a rigid layer of block copolymer surrounding the surface of the cellulose nanocrystals, where PPO blocks are more proximal to the TOCNC surface, is more likely.

QCM-D data presented in Figs. 7 and S4 indicate slow and mainly irreversible adsorption of F127 on TOCNC, resulting in a formation of a thin and rigid layer of block copolymer around the nanocrystals. The Δf

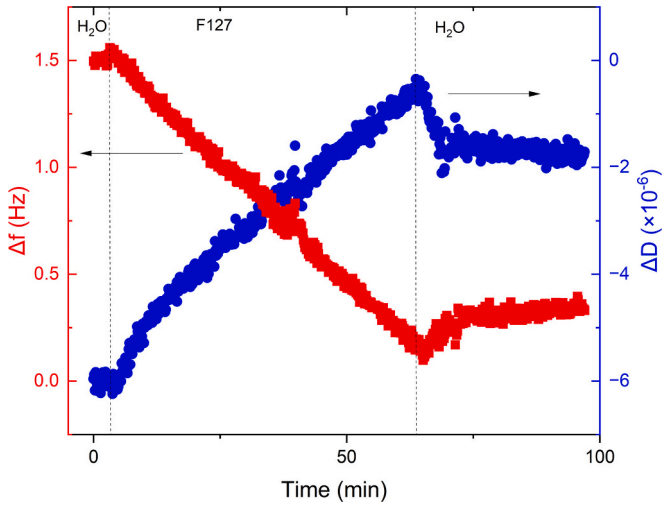

Fig. 7. Changes in resonance frequency (Δf) and dissipation (ΔD) (overtone n = 5) as a function of time for adsorption of 100 mg/l F127 and subsequent rinsing with water on TOCNC.

value for a polymer layer formed during one-hour period of adsorption and subsequent rinsing with water was -3.6 ± 1.6 Hz, corresponding to 640 $\pm$ 280 ng m^{-2} of polymer on the surface (calculated using the Sauerbrey equation, Eq. (5)). As expected, the adsorbed and very thin polymer layer does not affect the morphology of the of TOCNC film (Fig. S5).

Kushan and Senses (2021) studied the rheological properties of F127/CNC gel composites and reported that the adsorption of PPO blocks onto CNCs might be favoured only when the temperature is increased above the critical micellization temperature. They argued that, up to a CNC concentration of 3 wt%, the adsorption of PPO blocks is favourable with increasing temperature. In the present study, however, all the conditions were carefully selected to remain below the critical micellization temperature and a defined concentration of F127 (CMT = 27 °C at 1 wt%). Still, all the evidence suggests that adsorption of F127 onto cellulose surfaces seems to be preceded by PPO blocks even at low temperatures, and not by a bridging mechanism of PEO to CNC as suggested in earlier reports (Li et al., 2012; Nagalakshmaiah et al., 2016). Our findings corroborate those of Reid et al. (2017), even though their work focused on the adsorption of PEG copolymers. Holappa et al. (2013) studied the adsorption of hydrophobically end-capped PEG on cellulose and silica below the critical association concentration – that is, the point at which the premicellar aggregates are formed (Szutkowski et al., 2018). Hydrophilic silica attracts PEG by polar interactions between the oxygen groups of PEG and OH groups on the silica surface (Holappa et al., 2013). Adsorption of PEG onto cellulose was, however, found to be low, due to the amphiphilic nature of cellulose and due to its inherent lack of affinity with PEG. It is also important to highlight that, despite our TOCNC having an abundance of hydroxy groups theoretically available for PEO-TOCNC interactions to occur, PPO blocks are still spatially closer to the TOCNC surface. This further proves that adsorption is likely to occur. However, this adsorption is more likely to occur simply due to the formation of a layer of F127 on the surface of TOCNC.

3.4. Thermal analysis

The thermal stability of the samples was evaluated by thermogravimetric analysis (TGA). Fig. 8a presents these data as mass loss of the samples as a function of an increase in temperature. Overall, little variation was seen for the onset of thermal degradation of SCNC,

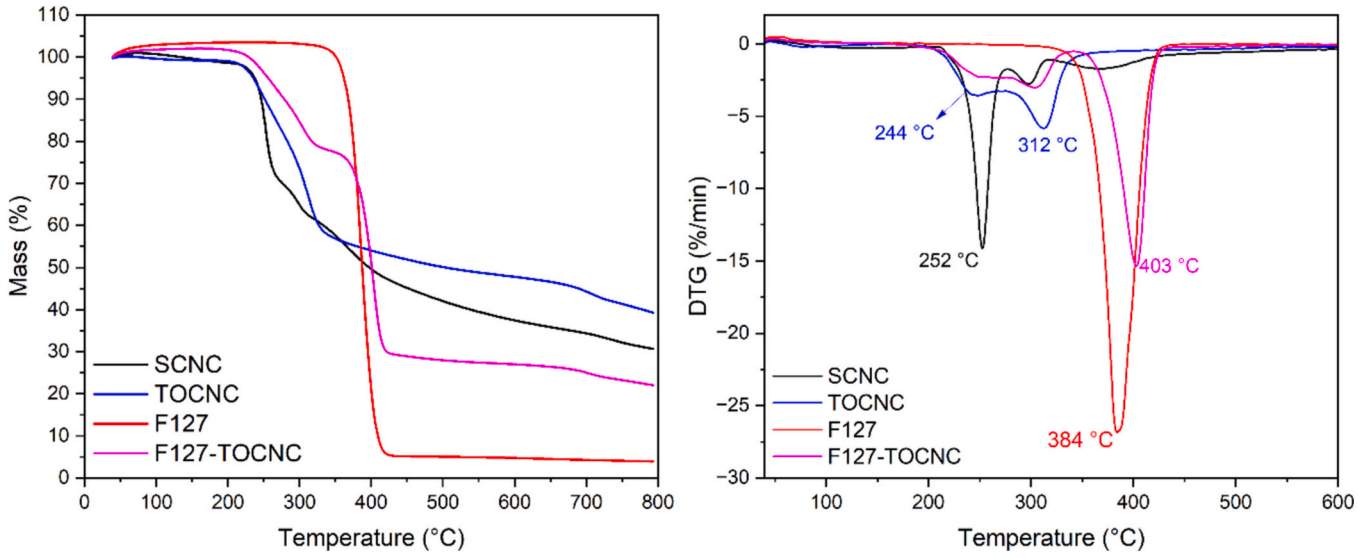

Fig. 8. Thermal Gravimetric Analysis (TGA) (a) and Differential Thermal Gravimetry (DTG) (b) thermograms of sulfated CNCs (SCNC), TEMPO-oxidised CNCs (TOCNC), Pluronic F127 poloxamer (F127) and F127 modified TOCNC (F127-TOCNC).

TOCNC, and their F127-modified counterparts. F127 block copolymer, on the other hand, showed a single mass loss event, with an onset degradation temperature of ~390 °C related to the thermal depolymerization of PEO and PPO blocks (Dou et al., 2016). For CNC samples, more events can be identified from the derivative of the mass loss in Fig. 8b. SCNC exhibits a derivative peak at ~252 °C, which relates to the early degradation of anhydroglucoronate units with sulfate half-ester groups. The remaining unmodified units in SCNCs then degrade at ~296 °C. Similarly, TOCNC exhibits a degradation peak at ~244 °C related to carboxylate anhydroglucoronate groups, and unmodified glucose units then exhibited a degradation event at 312 °C (Fukuzumi et al., 2010; Lavoine et al., 2016). F127-TOCNC exhibits two early degradation events that could be related to unmodified cellulose chains, that is, where the block copolymer did not fully adsorb. The main degradation event, however, occurred at 403 °C which was 19 °C higher than that of the neat block copolymer. This is indicative of aggregation between F127 and TOCNC or a protective effect of F127 surrounding TOCNC – as confirmed by AFM and QCM-D results – in which F127 is densely packed around the CNCs. This phenomenon has been observed for hydrophobically-capped polyethylene glycol block copolymers adsorbed onto cellulose surfaces (Holappa et al., 2013). Nevertheless, this could be advantageous for the use of F127-TOCNCs in polymer composites requiring high processing temperatures or for the application of F127 modified CNCs in sensors.

Differential scanning calorimetry (DSC) was performed to evaluate the crystallization, enthalpy, and phase transitions of F127 and F127-TOCNC. Fig. 9 shows the heat flow thermograms of the first heat run for all samples. Notably, SCNC and TOCNC exhibit broad endothermic peaks. Since CNCs do not exhibit any glass transition or melting point, the enthalpy values obtained could be related to water evaporation events during the first heating cycle (Rasri et al., 2023).

Pluronic triblock copolymers of the F127 kind undergo a phase transition from its unimer to its micelle form, which can be identified from the centre of the melting peak located at ~56 °C. At high concentrations, these poloxamers self-assemble into core-shell micelles and exhibit liquid-crystalline phases (Cohen et al., 2020). Here, the introduction of TOCNC to F127 caused a reduction in both the phase transition temperature and crystallinity of F127. When comparing neat F127 to F127-TOCNC, a significant reduction in enthalpy was observed - from 109.9 J g^{-1} to 56.6 J g^{-1}, respectively. TOCNC leads to a reduction in the energy needed for self-assembly formation due to the interaction of PPO blocks with the CNCs. Additionally, the crystallinity of F127 was

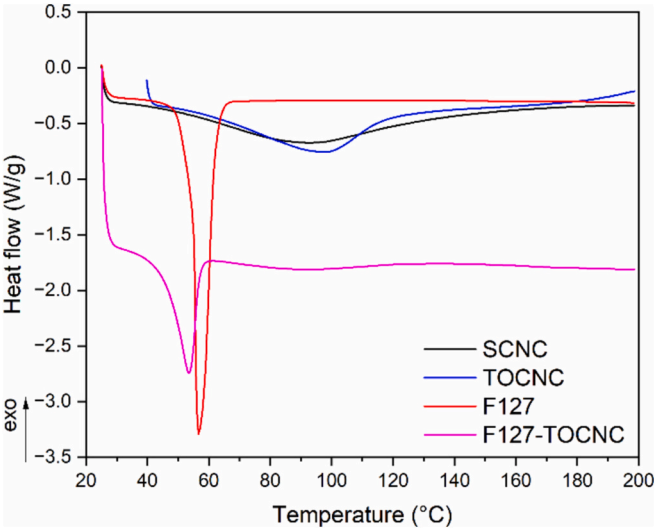

Fig. 9. Typical Differential Scanning Calorimetry (DSC) thermograms of sulfated CNCs (SCNC), TEMPO-oxidised CNCs (TOCNC), Pluronic F127 poloxamer (F127) and F127 modified TOCNC (F127-TOCNC).

significantly reduced when adsorbed onto the TOCNC surfaces. In the case of nonionic block copolymers and their ability to self-assemble, it is possible that the presence of F127-adsorbed CNC could have a hindering effect in the self-assembly of F127, thus leading to lower crystallinity when compared to neat F127 or F127 solutions. Since the properties of pluronics are also highly dependent on temperature and concentration to promote gelation, it is unlikely that a 1 wt% suspension would lead to gel formation for being below the critical micelle concentration (CMC) of F127. Still, these DSC data appear to capture this effect.

A transition temperature (as calculated from the DSC melting peak) of ~56 °C was observed for neat F127 – well above the temperature in which the mixing carried out (4 °C). This should, according to Tarhanlı and Senses (2023), favour adsorption of PEO blocks. That, however, did not occur. In this sense, the observations made by Reid et al. (2017) on PEG adsorption to cellulose surfaces seem to support our findings: no evidence of hydrogen bonding through NMR was found even for F127, though intimate adsorption seems to occur. This leads us to believe that PPO blocks, being closer to the TOCNC surface, did not form an anchor-

buoy-anchor type of bridge, but instead seem to be surrounding the surface of TOCNC intimately, driving PEO brushes further away from them, forming a rigid layer of block copolymer around the TOCNCs.

3.5. Rheological properties

The viscosities of the samples (Fig. 10) were evaluated using 10 wt% suspensions. All samples exhibit shear thinning behaviour with an increase in the shear rate, which is typical for both CNC and F127 aqueous solutions at 10–20 wt% concentrations (Gicquel et al., 2019; Jiang et al., 2019; Shriky et al., 2020). F127 formed a gel at 25 °C and at a concentration of 10 wt%, which is in line with reports that this poloxamer can gel when the concentration is above the CMC (Liu & Li, 2015; Russo et al., 2024).

Overall, TEMPO oxidation did not effect the viscosity of SCNC samples. F127 displayed the highest viscosity of all samples due to its capacity to form an organized structure above its CMC (Suman et al., 2021). When F127 was added to TOCNC, the intermicellar interactions were disrupted by the presence of the nanocrystals, resulting in a weaker gel with a lower viscosity. This disruption is also thought to be linked to the adsorption of F127 onto CNC (Kushan & Senses, 2021). Still, the viscosity increased in comparison to TOCNC, showing that F127 could possibly aid the gelation of nanocrystal suspensions. As such, this is further evidence that adsorption persists in aqueous media.

4. Conclusions

The surface oxidation of SCNCs using TEMPO was achieved, and the subsequent adsorption of F127 to the surfaces of TOCNCs. F127 was found to remain in a unimer form in aqueous suspensions. Our findings suggest that adsorption occurs by the formation of a rigid layer of block copolymer surrounding the TOCNC, where PPO blocks are more proximal to TOCNC. In addition, PPO adsorption to TOCNC happened regardless of the suspensions being above the Critical Micelle Temperature (CMT). SS-NMR experiments, which were performed on freeze-dried samples, pointed to PPO blocks being more proximal to the TOCNC surfaces. QCM-D and AFM evidenced the formation of a thin layer of block copolymer surrounding the TOCNC, confirming the adsorption. This adsorption has been shown to be persistent even after subsequent solubilisation.

The findings of this work could be further explored in subsequent experiments in the presence and in the absence of water to better understand how poloxamers interact with cellulose surfaces. In summary, we emphasise the importance of understanding the complexity of cellulose and water interactions, and to examine the effects of the nanoparticles' medium on nonionic polymer adsorption behaviour, particularly for the processing of composite gels. In addition to that, we call for more experimental and theoretical studies to fully understand the nature of adsorption of this class of block copolymers.

CRediT authorship contribution statement

Alessandra Lavoratti: Writing – review & editing, Writing – original draft, Visualization, Validation, Methodology, Investigation, Formal analysis, Data curation, Conceptualization. **Onajite Abafe Diejomaoh:** Writing – review & editing, Validation, Investigation, Formal analysis. **Annela M. Seddon:** Writing – review & editing, Supervision, Methodology, Formal analysis, Data curation. **Todor T. Koev:** Writing – review & editing, Visualization, Validation, Resources, Investigation, Formal analysis, Data curation. **Yaroslav Z. Khimyak:** Writing – review & editing, Methodology, Funding acquisition, Formal analysis. **Robert L. Harniman:** Writing – review & editing, Data curation, Investigation, Formal analysis. **Katri S. Kontturi:** Validation, Software, Methodology, Investigation, Formal analysis, Data curation. **Tekla Tammelin:** Supervision, Methodology, Funding acquisition, Formal analysis, Data curation. **Stephen J. Eichhorn:** Writing – review & editing, Validation, Supervision, Project administration, Methodology, Funding acquisition, Formal analysis, Conceptualization.

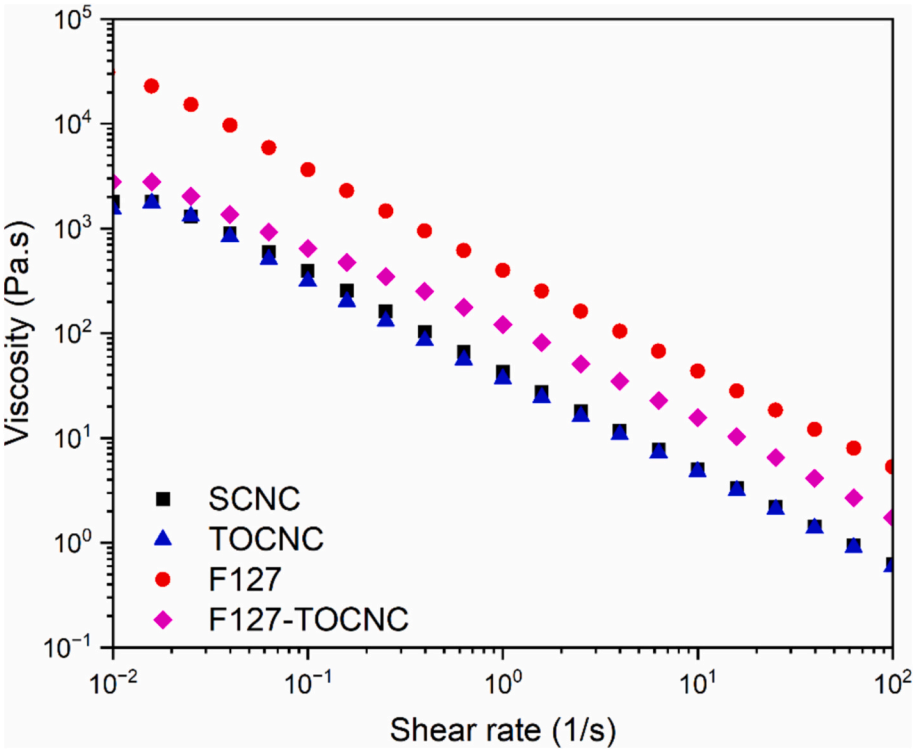

Fig. 10. Typical viscosity versus shear rate data for sulfated CNCs (SCNC), TEMPO-oxidised CNCs (TOCNC), Pluronic F127 poloxamer (F127) and F127 modified TOCNC (F127-TOCNC).

Declaration of competing interest

None.

Acknowledgements

S.J.E., A.L., and O.A.D. would like to thank the Engineering and Physical Sciences Research Council (EPSRC), Grant No. EP/V002651/1, for funding. Electron microscope studies were carried out in the Chemical Imaging Facility at the University of Bristol by Dr. Jean-Charles Eloi. The Ganesha X-ray scattering apparatus used for this research was purchased under EPSRC Grant 'Atoms to Applications' Grant ref. EP/K035746/1. This work benefited from SasView software, originally developed by the DANSE project under NSF award DMR-0520547. The authors also grateful to the University of East Anglia's Faculty of Science NMR facility and to the HH Wills Physics Laboratory for the SAXS experiments. T.K. is funded via a UKRI Future Leaders Fellowship awarded to Dr. Matthew Wallace (MR/T044020/1). K.S.K. acknowledges Research Council of Finland project PreDesign (no. 361951) for funding. T.T. acknowledges Research Council of Finland Flagship Program FinnCERES (no. 318890 and 318891) for funding.

Appendix A. Supplementary data

Supplementary data to this article can be found online at https://doi.org/10.1016/j.carbpol.2024.123156.

Data availability

Data will be made available on request.

References

Alqus, R., Eichhorn, S. J., & Bryce, R. A. (2015). Molecular dynamics of cellulose amphiphilicity at the graphene-water interface. *Biomacromolecules, 16*(6), 1771–1783. https://doi.org/10.1021/ACS.BIOMAC.5B00307/SUPPL_FILE/BM5B00307_SI_001.PDF

Arranja, A., Denkova, A. G., Morawska, K., Waton, G., Van Vlierberghe, S., Dubruel, P., … Mendes, E. (2016). Interactions of Pluronic nanocarriers with 2D and 3D cell cultures: Effects of PEO block length and aggregation state. *Journal of Controlled Release, 224*, 126–135. https://doi.org/10.1016/J.JCONREL.2016.01.014

Arumughan, V., Nypelö, T., Hasani, M., & Larsson, A. (2021). Fundamental aspects of the non-covalent modification of cellulose via polymer adsorption. In *, vol. 298*. *Advances in colloid and interface science*. Elsevier B.V. https://doi.org/10.1016/j.cis.2021.102529.

Bardet, R., Belgacem, N., & Bras, J. (2015). Flexibility and color monitoring of cellulose nanocrystal iridescent solid films using anionic or neutral polymers. *ACS Applied Materials and Interfaces, 7*(7), 4010–4018. https://doi.org/10.1021/am506786t

Batta-Mpouma, J., Kandhola, G., & Kim, J. W. (2023). Ionically crosslinked cellulose nanocrystals by metal nitrates for the preparation of stable emulsions with tunable interface properties. *Scientific Reports 2023 13:1, 13*(1), 1–15. https://doi.org/10.1038/s41598-023-48703-3

Bertula, K., Martikainen, L., Munne, P., Hietala, S., Klefström, J., Ikkala, O., & Nonappa.. (2019). Strain-stiffening of agarose gels. *ACS Macro Letters, 8*(6), 670–675. https://doi.org/10.1021/acsmacrolett.9b00258

Boonrat, O., Tantishaiyakul, V., Hirun, N., Rugmai, S., & Soontaranon, S. (2021). Structural characterization using SAXS and rheological behaviors of pluronic F127 and methylcellulose blends. *Polymer Bulletin, 78*(3), 1175–1187. https://doi.org/10.1007/S00289-020-03154-Y/FIGURES/5

Branca, C., & D'Angelo, G. (2019). Aggregation behavior of pluronic F127 solutions in presence of chitosan/clay nanocomposites examined by dynamic light scattering. *Journal of Colloid and Interface Science, 542*, 289–295. https://doi.org/10.1016/J.JCIS.2019.02.031

Builes, D. H., Labidi, J., Eceiza, A., Mondragon, I., & Tercjak, A. (2013). Unsaturated polyester nanocomposites modified with fibrillated cellulose and PEO-b-PPO-b-PEO block copolymer. *Composites Science and Technology, 89*, 120–126. https://doi.org/10.1016/J.COMPSCITECH.2013.09.015

Carrera Espinoza, M. J., Lin, K. S., Weng, M. T., Kunene, S. C., Wang, S.-S., & S.. (2021). In vitro studies of Pluronic F127 coated magnetic silica nanocarriers for drug delivery system targeting liver cancer. *European Polymer Journal, 153*. https://doi.org/10.1016/j.eurpolymj.2021.110504

Cheng, D., Wen, Y., Wang, L., An, X., Zhu, X., & Ni, Y. (2015). Adsorption of polyethylene glycol (PEG) onto cellulose nano-crystals to improve its dispersity. *Carbohydrate Polymers, 123*, 157–163. https://doi.org/10.1016/j.carbpol.2015.01.035

Cohen, N., Attia, D., Levi-Kalisman, Y., Bitton, R., & Yerushalmi-Rozen, R. (2022). Emergent hybrid mesophases in ternary mixtures of cellulose nanocrystals - Pluronic micelles-water. *Polymers for Advanced Technologies, 33*(11), 3800–3809. https://doi.org/10.1002/PAT.5647

Cohen, N., Ochbaum, G., Levi-Kalisman, Y., Bitton, R., & Yerushalmi-Rozen, R. (2020). Polymer-induced modification of cellulose nanocrystal assemblies in aqueous suspensions. *ACS Applied Polymer Materials, 2*(2), 732–740. https://doi.org/10.1021/acsapm.9b01048

Cohen-Erner, M., Khandadash, R., Hof, R., Shalev, O., Antebi, A., Cyjon, A., … Peer, D. (2021). Fe3O4Nanoparticles and paraffin wax as phase change materials embedded in polymer matrixes for temperature-controlled magnetic hyperthermia. *ACS Applied Nano Materials, 4*(10), 11187–11198. https://doi.org/10.1021/acsanm.1c02676

Dou, Q., Karim, A. A., & Loh, X. J. (2016). Modification of thermal and mechanical properties of PEG-PPG-PEG copolymer (F127) with MA-POSS. *Polymers, 8*(9), 341. https://doi.org/10.3390/POLYM8090341

Eichhorn, S. J., Etale, A., Wang, J., Berglund, L. A., Li, Y., Cai, Y., … Frka-Petesic, B. (2022). Current international research into cellulose as a functional nanomaterial for advanced applications. *Journal of Materials Science 2022 57:10, 57*(10), 5697–5767. https://doi.org/10.1007/S10853-022-06903-8

Etale, A., Onyianta, A. J., Turner, S. R., & Eichhorn, S. J. (2023). Cellulose: A review of water interactions, applications in composites, and water treatment. In *Chemical reviews (Vol. 123, Issue 5, pp. 2016–2048)*. American Chemical Society. https://doi.org/10.1021/acs.chemrev.2c00477.

Foster, E. J., Moon, R. J., Agarwal, U. P., Bortner, M. J., Bras, J., Camarero-Espinosa, S., … Youngblood, J. (2018). Current characterization methods for cellulose nanomaterials. In *Chemical society reviews (Vol. 47, Issue 8, pp. 2609–2679)*. Royal Society of Chemistry. https://doi.org/10.1039/c6cs00895j.

Fraschini, C., Chauve, G., & Bouchard, J. (2017). TEMPO-mediated surface oxidation of cellulose nanocrystals (CNCs). *Cellulose, 24*(7), 2775–2790. https://doi.org/10.1007/s10570-017-1319-5

Fukuzumi, H., Saito, T., Okita, Y., & Isogai, A. (2010). Thermal stabilization of TEMPO-oxidized cellulose. *Polymer Degradation and Stability, 95*(9), 1502–1508. https://doi.org/10.1016/J.POLYMDEGRADSTAB. 2010.06.015

Gicquel, E., Martin, C., Gauthier, Q., Engström, J., Abbattista, C., Carlmark, A., … Bras, J. (2019). Tailoring rheological properties of thermoresponsive hydrogels through block copolymer adsorption to cellulose nanocrystals. *Biomacromolecules, 20*(7), 2545–2556. https://doi.org/10.1021/acs.biomac.9b00327

Gomez-Hermoso-de-Mendoza, J., Gutierrez, J., & Tercjak, A. (2023). Highly hydrophobic cellulose acetate mats modified with poly(ethylene oxide-b-propylene oxide-b-ethylene oxide) triblock copolymer and TiO2 nanoparticles by electrospinning. *Cellulose, 30*(15), 9501–9515. https://doi.org/10.1007/S10570-023-05417-Z/FIGURES/5

Gutierrez, J., Carrasco-Hernandez, S., Barud, H. S., Oliveira, R. L., Carvalho, R. A., Amaral, A. C., & Tercjak, A. (2017). Transparent nanostructured cellulose acetate films based on the self assembly of PEO-b-PPO-b-PEO block copolymer. *Carbohydrate Polymers, 165*, 437–443. https://doi.org/10.1016/J.CARBPOL.2017.02.070

Habibi, Y., Chanzy, H., & Vignon, M. R. (2006). TEMPO-mediated surface oxidation of cellulose whiskers. *Cellulose, 13*(6), 679–687. https://doi.org/10.1007/s10570-006-9075-y

Hanus, J., & Mazeau, K. (2006). The xyloglucan–cellulose assembly at the atomic scale. *Biopolymers, 82*(1), 59–73. https://doi.org/10.1002/BIP.20460

Holappa, S., Kontturi, K. S., Salminen, A., Seppälä, J., & Laine, J. (2013). Adsorption of hydrophobically end-capped poly(ethylene glycol) on cellulose. *Langmuir, 29*(45), 13750–13759. https://doi.org/10.1021/LA402494M/SUPPL_FILE/LA402494M_SI_001.PDF

Isogai, A., Saito, T., & Fukuzumi, H. (2011). TEMPO-oxidized cellulose nanofibers. In *Nanoscale (vol. 3, issue 1, pp. 71–85)*. https://doi.org/10.1039/c0nr00583e

Jiang, Z., Tang, L., Gao, X., Zhang, W., Ma, J., & Zhang, L. (2019). Solvent regulation approach for preparing cellulose-nanocrystal-reinforced regenerated cellulose fibers and their properties. *ACS Omega, 4*(1), 2001–2008. https://doi.org/10.1021/acsomega.8b03601

Khaliq, N. U., Lee, J., Kim, S., Sung, D., & Kim, H. (2023). Pluronic F-68 and F-127 based nanomedicines for advancing combination cancer therapy. *Pharmaceutics, 15*(8), 2102. https://doi.org/10.3390/PHARMACEUTICS15082102

Kim, H., Endrődi, B., Salazar-Alvarez, G., & Cornell, A. (2019). One-step electro-precipitation of nanocellulose hydrogels on conducting substrates and its possible applications: Coatings, composites, and energy devices. *ACS Sustainable Chemistry and Engineering, 7*(24), 19415–19425. https://doi.org/10.1021/acssuschemeng.9b04171

Kong, L., Alqus, R., Yong, C. W., Todorov, I., Eichhorn, S. J., & Bryce, R. A. (2023). Cellulose Iβ microfibril interaction with pristine graphene in water: Effects of amphiphilicity by molecular simulation. *Journal of Molecular Graphics and Modelling, 118*, Article 108336. https://doi.org/10.1016/J.JMGM.2022.108336

Kumar, K., Umapathi, R., & Venkatesu, P. (2023). Ionic liquids mediated micellization of pluronic copolymers: Aggregation behavior of amphiphilic triblock copolymers. In *Journal of physical chemistry B (vol. 127, issue 10, pp. 2107–2120)*. American Chemical Society. https://doi.org/10.1021/acs.jpcb.2c05683.

Kushan, E., & Senses, E. (2021). Thermoresponsive and injectable composite hydrogels of cellulose nanocrystals and Pluronic F127. *ACS Applied Bio Materials, 4*(4), 3507–3517. https://doi.org/10.1021/acsabm.1c00046

Lavoine, N., Bras, J., Saito, T., Isogai, A., Lavoine, N., Saito, T., … Bras, J. (2016). Improvement of the thermal stability of TEMPO-oxidized cellulose nanofibrils by heat-induced conversion of ionic bonds to amide bonds. *Macromolecular Rapid Communications, 37*(13), 1033–1039. https://doi.org/10.1002/MARC.201600186

Li, B., Xu, W., Kronlund, D., Määttänen, A., Liu, J., Smått, J. H., … Xu, C. (2015). Cellulose nanocrystals prepared via formic acid hydrolysis followed by TEMPO-mediated oxidation. *Carbohydrate Polymers, 133*, 605–612. https://doi.org/10.1016/j.carbpol.2015.07.033

Li, T., Zhong, Q., Zhao, B., Lenaghan, S., Wang, S., & Wu, T. (2020). Effect of surface charge density on the ice recrystallization inhibition activity of nanocelluloses. *Carbohydrate Polymers, 234*. https://doi.org/10.1016/j.carbpol.2020.115863

Li, Y., Liu, H., Song, J., Rojas, O. J., & Hinestroza, J. P. (2011). Adsorption and association of a symmetric PEO-PPO-PEO triblock copolymer on polypropylene, polyethylene, and cellulose surfaces. *ACS Applied Materials and Interfaces, 3*(7), 2349–2357. https://doi.org/10.1021/am200264r

Li, Y., Rojas, O. J., & Hinestroza, J. P. (2012). Boundary lubrication of PEO-PPO-PEO triblock copolymer physisorbed on polypropylene, polyethylene, and cellulose surfaces. *Industrial and Engineering Chemistry Research, 51*(7), 2931–2940. https://doi.org/10.1021/ie202292r

Liu, S., & Li, L. (2015). Molecular interactions between PEO-PPO-PEO and PPO-PEO-PPO triblock copolymers in aqueous solution. *Colloids and Surfaces A: Physicochemical and Engineering Aspects, 484*, 485–497. https://doi.org/10.1016/j.colsurfa.2015.08.034

Llàcer Navarro, S., Nakayama, K., Idström, A., Evenäs, L., Ström, A., & Nypelö, T. (2021). The effect of sulfate half-ester groups on cellulose nanocrystal periodate oxidation. *Cellulose, 28*(15), 9633–9644. https://doi.org/10.1007/s10570-021-04115-y

Mata, J., Joshi, T., Varade, D., Ghosh, G., & Bahadur, P. (2004). Aggregation behavior of a PEO-PPO-PEO block copolymer + ionic surfactants mixed systems in water and aqueous salt solutions. *Colloids and Surfaces A: Physicochemical and Engineering Aspects, 247*(1–3), 1–7. https://doi.org/10.1016/j.colsurfa.2004.07.011

Nagalakshmaiah, M., Pignon, F., El Kissi, N., & Dufresne, A. (2016). Surface adsorption of triblock copolymer (PEO-PPO-PEO) on cellulose nanocrystals and their melt extrusion with polyethylene. *RSC Advances, 6*(70), 66224–66232. https://doi.org/10.1039/c6ra11139d

Ojha, J., Nanda, R., & Dorai, K. (2020). NMR investigation of the thermogelling properties, anomalous diffusion, and structural changes in a Pluronic F127 triblock copolymer in the presence of gold nanoparticles. *Colloid and Polymer Science, 298*(11), 1571–1585. https://doi.org/10.1007/S00396-020-04740-2/FIGURES/3

Onyianta, A. J., Etale, A., Koev, T. T., Eloi, J. C., Khimyak, Y. Z., & Eichhorn, S. J. (2022). Amphiphilic cellulose nanocrystals for aqueous processing of thermoplastics. *ACS Applied Polymer Materials, 4*(11), 8684–8693. https://doi.org/10.1021/ACSAPM.2C01623/ASSET/IMAGES/LARGE/AP2C01623_0011.JPEG

Onyianta, A. J., Xu, G., Etale, A., Eloi, J. C., & Eichhorn, S. J. (2023). Tackling the challenge of drying and redispersion of cellulose nanofibrils via membrane-facilitated liquid phase exchange. *Carbohydrate Polymers, 314*. https://doi.org/10.1016/j.carbpol.2023.120943

Orasugh, J. T., Dutta, S., Das, D., Pal, C., Zaman, A., Das, S., … Chattopadhyay, D. (2019). Sustained release of ketorolac tromethamine from poloxamer 407/cellulose nanofibrils graft nanocollagen based ophthalmic formulations. *International Journal of Biological Macromolecules, 140*, 441–453. https://doi.org/10.1016/J.IJBIOMAC.2019.08.143

Rasri, W., Thu, V. T., Corpuz, A., & Nguyen, L. T. (2023). Preparation and characterization of cellulose nanocrystals from corncob via ionic liquid [Bmim][HSO4] hydrolysis: Effects of major process conditions on dimensions of the product. *RSC Advances, 13*(28), 19020–19029. https://doi.org/10.1039/D3RA02715E

Reid, M. S., Villalobos, M., & Cranston, E. D. (2017). The role of hydrogen bonding in non-ionic polymer adsorption to cellulose nanocrystals and silica colloids. In *Current opinion in colloid and interface science (vol. 29, pp. 76–82)*. Elsevier Ltd.. https://doi.org/10.1016/j.cocis.2017.03.005

Russo, G., Rossella Delpiano, G., Carucci, C., Grosso, M., Dessì, C., Söderman, O., Lindman, B., Monduzzi, M., & Salis, A. (2024). Tuning Pluronic F127 phase transitions by adding physiological amounts of salts: A rheology, SAXS, and NMR investigation. *European Polymer Journal, 204*, Article 112714. https://doi.org/10.1016/J.EURPOLYMJ.2023.112714

Sarkar, B., & Alexandridis, P. (2012). Self-assembled block copolymer-nanoparticle hybrids: Interplay between enthalpy and entropy. *Langmuir, 28*(45), 15975–15986. https://doi.org/10.1021/LA303568E/ASSET/IMAGES/LARGE/LA-2012-03568E_0007.JPEG

Sauerbrey, G. (1959). Verwendung von Schwingquarzen zur Wägung dünner Schichten und zur Mikrowägung. *Zeitschrift für Physik, 155*(2), 206–222. https://doi.org/10.1007/BF01337937/METRICS

Shaker, M. A., Elbadawy, H. M., & Shaker, M. A. (2020). Improved solubility, dissolution, and oral bioavailability for atorvastatin-Pluronic® solid dispersions. *International Journal of Pharmaceutics, 574*. https://doi.org/10.1016/j.ijpharm.2019.118891

Shriky, B., Kelly, A., Isreb, M., Babenko, M., Mahmoudi, N., Rogers, S., Shebanova, O., Snow, T., & Gough, T. (2020). Pluronic F127 thermosensitive injectable smart hydrogels for controlled drug delivery system development. *Journal of Colloid and Interface Science, 565*, 119–130. https://doi.org/10.1016/j.jcis.2019.12.096

Solhi, L., Guccini, V., Heise, K., Solala, I., Niinivaara, E., Xu, W., … Kontturi, E. (2023). Understanding Nanocellulose-water interactions: Turning a detriment into an asset. In *Chemical reviews (vol. 123, issue 5, pp. 1925–2015)*. American Chemical Society. https://doi.org/10.1021/acs.chemrev.2c00611.

Suhail, M., Hung, M. C., Chiu, I. H., Vu, Q. L., & Wu, P. C. (2022). Preparation and in-vitro characterization of 5-aminosalicylic acid loaded hydrogels for colon specific delivery. *Journal of Materials Research and Technology, 21*, 339–352. https://doi.org/10.1016/j.jmrt.2022.09.031

Suman, K., Sourav, S., & Joshi, Y. M. (2021). Rheological signatures of gel-glass transition and a revised phase diagram of an aqueous triblock copolymer solution of Pluronic F127. *Physics of Fluids, 33*(7). https://doi.org/10.1063/5.0057090/1076889

Szutkowski, K., Kołodziejska, Z., Pietralik, Z., Zhukov, I., Skrzypczak, A., Materna, K., & Kozak, M. (2018). Clear distinction between CAC and CMC revealed by high-resolution NMR diffusometry for a series of bis-imidazolium gemini surfactants in aqueous solutions. *RSC Advances, 8*(67), 38470–38482. https://doi.org/10.1039/C8RA07081D

Tarhanlı, İ., & Senses, E. (2023). Cellulose nanocrystal and Pluronic L121-based thermo-responsive composite hydrogels. *Carbohydrate Polymers, 321*. https://doi.org/10.1016/j.carbpol.2023.121281

Tenorio-Alfonso, A., Vázquez Ramos, E., Martínez, I., Ambrosi, M., & Raudino, M. (2023). Assessment of the structures contribution (crystalline and mesophases) and mechanical properties of polycaprolactone/pluronic blends. *Journal of the Mechanical Behavior of Biomedical Materials, 139*. https://doi.org/10.1016/j.jmbbm.2023.105668

Tercjak, A., Gutierrez, J., Barud, H. S., Domeneguetti, R. R., & Ribeiro, S. J. L. (2015). Nano- and macroscale structural and mechanical properties of in situ synthesized bacterial cellulose/PEO-b-PPO-b-PEO biocomposites. *ACS Applied Materials and Interfaces, 7*(7), 4142–4150. https://doi.org/10.1021/AM508273X/ASSET/IMAGES/LARGE/AM-2014-08273X_0009.JPEG

Vanderfleet, O. M., Reid, M. S., Bras, J., Heux, L., Godoy-Vargas, J., Panga, M. K. R., & Cranston, E. D. (2019). Insight into thermal stability of cellulose nanocrystals from new hydrolysis methods with acid blends. *Cellulose, 26*(1), 507–528. https://doi.org/10.1007/S10570-018-2175-7